RADC-TR-73-343
Final Technical Report
September 1973

OBSERVATION OF STAR-PAIR IMAGES FOR ESTIMATION OF ISOPLANATIC PATCH SIZE IN THE ATMOSPHERE

Federal Scientific Corporation

AF30602-73-C-0284

Sponsored by
Defense Advanced Research Projects Agency
ARPA Order No. 1279

Rome Air Development Center
Air Force Systems Command
Griffiss Air Force Base, New York

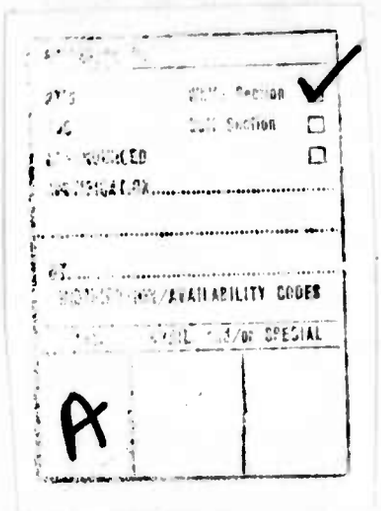

OBSERVATION OF STAR-PAIR IMAGES FOR ESTIMATION OF ISOPLANATIC PATCH SIZE IN THE ATMOSPHERE

T. W. Parsons

Contractor: Federal Scientific Corporation
Contract Number: F30602-73-C-0284
Effective Date of Contract: 12 February 1973
Expiration Date of Contract: 12 September 1973
Amount of Contract: $30,000.00
Program Code Number: 3E20

Principal Investigator: Thomas M. Parsons
Phone: 212 286-4400

Contract Engineer: Donald Hanson
Phone: 315 330-3145

Project Engineer: Mark R. Weiss
Phone: 212 286-4400

This research was supported by the Defense Advanced Research Projects Agency of the Department of Defense and was monitored by Donald W. Hanson, RADC (OCSA), GAFB, NY 13440 under contract F30602-73-C-0284.

PUBLICATION REVIEW

This technical report has been reviewed and is approved

Donald W. Hanson

RADC Project Engineer

ABSTRACT

An experiment is described which attempts to measure the isoplanatic patch size of the atmosphere as a function of various parameters. Technique constraints and the data analysis procedures used are described and results are discussed. It is shown that the constraints in data collection impaired the data analysis and prevented a measurement of the isoplanatic patch size. Recommendations are given for getting better data in the future.

CONTENTS

LIST OF FIGURES

LIST OF TABLES

1.0 SUMMARY

The purpose of this project is to estimate the isoplanatic patch size of the atmosphere as a function of elevation angle, meteorological conditions, and possibly other variables. The concept of the isoplanatic patch is discussed in reference 1. Briefly, a region of the atmosphere is termed an isoplanatic patch if the optical characteristics of the atmosphere are essentially uniform over the region.

The method of measurement is as follows: Pairs of stars are selected which have separations ranging from a few seconds of arc to over 200 seconds of arc. Since stars are approximately point sources, the image of each star is the point-spread function (PSF) of the atmosphere/telescope channel through which it is viewed. If the two images are alike, they lie within an isoplanatic region. The test of similarity of images is the degree of success with which one image can be used to restore the other image by deconvolution. The quality of restoration is measured by the width of the image before and after processing. By processing a sufficient number of star-pair images and observing the degree of similarity as a function of separation, it should be possible to estimate the probability that a patch of a given size will be isoplanatic. The role of Federal Scientific Corporation in this project was to develop data-reduction procedures for evaluating the input data, doing the image restoration, and evaluating the success of the restoration, and to perform the reduction. In addition, we have presented some basic relationships which

give some idea of the limitations of the restoration process and the tradeoffs permitted. This background helps in judging the restoration results intelligently.

In analyzing the results of the experiment, we determined that the data provided to us for processing were unsatisfactory, chiefly because the star pairs had been photographed with too long an exposure, but possibly also because of scattering of light within the emulsion of the film. As a result, most of the images tended toward the Gaussian shape, regardless of the separation between the stars, and it was impossible to tell whether the two stars had been inside an isoplanatic patch or not.

Further research should be done using shorter exposures and, if possible, thinner emulsions. It is possible that the range of available photographic media for this purpose has not been fully explored. Alternate imaging methods (e.g., vidicons) should also be investigated.

2.0 THEORETICAL STUDIES

2.1 Width Improvement

In the following discussion, we assume familiarity with the general idea of image restoration by division of Fourier transforms. (Refs. 2, 3, 4.)

Let the point-spread function (PSF) of the atmosphere/telescope channel be $h(x,y)$, the blurred image $b(x,y)$ and the ideal image $p(x,y)$; let capitals denote Fourier transforms and F^{-1} indicate inverse transformation. Then, in the absence of noise, the ideal image can be recovered by means of the relation,

$$p(x,y) = F^{-1}\left[B(\xi,\eta)/H(\xi,\eta)\right] \tag{1}$$

assuming that at zeroes of H, the limit of B/H exists. In practice, both b and h are corrupted by noise. This can be haze or other scattered light in the atmosphere, fogging in the film, grain, or sampling noise. Some of this noise is additive and some not. If we assume it to be additive, we can write

$$d(x,y) = b(x,y) + n_b(x,y)$$

$$k(x,y) = h(x,y) + n_h(x,y)$$

Because of this noise, deconvolution by transform methods gives us only an estimate of p:

$$\hat{p}(x,y) = F^{-1}(D/K) = F^{-1}\left[\frac{B + N_b}{H + N_h}\right] \tag{2}$$

In practice, N_b and N_h are nearly uniform over the transform domain, while B and H fall off rapidly with increasing spatial frequency. As a result, the high-frequency regions of D/K are

extremely noisy and make little contribution to $\hat{p}$. It is customary to deal with this problem by some kind of low-pass filtering of D/K (see, for example, reference 3). It would be nice if we could design this filter to optimize the approximation of $\hat{p}$ to p in a mean-square sense. Analysis indicates, however, that such a filter has the effect of cancelling the inverse filter and replacing it with a minimum MSE filter. Since the object of the present experiment is to use success in inverse filtering as a measure of isoplanaticity, this replacement is not desirable. Instead, we use a simple rectangular filter:

$$G_o(\xi,\eta) = \begin{cases} 1, \sqrt{\xi^2+\eta^2} < R \\ 0 \quad \text{otherwise} \end{cases} \tag{3}$$

Then the restored image is

$$\hat{p}(x,y) = F^{-1}\left\{\frac{G_o(B+N_b)}{H+N_h}\right\} \tag{4}$$

Experience has shown that it is nearly always possible to reduce the apparent noise in $\hat{p}$ to any desired degree by choosing R sufficiently small. The resulting image, however, is convolved with g_o, the inverse transform of the filtering function, and as R decreases, the blurring effect of g_o may become worse than that of h, which we are trying to remove. Indeed, if R is chosen so that the transforms are virtually noise-free inside R, then the operation

$$\frac{G_o(B+N_o)}{H+N_i} \approx \frac{G_o B}{H} = \frac{G_o PH}{H} = G_o P,$$

essentially exchanges a new PSF (g_o) for the old one (h). Unless g_o is in some sense "tighter" than h, this is futile. In light of this, it is of interest to ask, for what value of R is the blurring effect of g_o worse than that of h?

The answer to this question depends on the shape of h and on the way in which we measure the blurring effect, or "width," of the PSF. For this analysis, we assume h Gaussian and centered at the origin, and measure width by the volume/height ratio,

$$W = \frac{\int_{-\infty}^{\infty}\int_{-\infty}^{\infty} f(x,y)\,dx\,dy}{f(0,0)} \tag{5}$$

(This is similar to the principal width measure used in the present project.)

If we assume circular symmetry, it is convenient to use Hankel transforms. Let r = radial distance and w = radial frequency. Then we have the following transform pairs:

PSF

$$h(r) = e^{-\frac{1}{2}\left(\frac{r}{\sigma_h}\right)^2} \longleftrightarrow H(w) = \sigma_h^2\, e^{-\frac{1}{2}(w\sigma_h)^2} \tag{6}$$

Filter

$$G(w) = \begin{cases} 1, & w < R \\ 0 & \text{otherwise} \end{cases} \longleftrightarrow g(r) = R\,\frac{J_1(Rr)}{r} \tag{7}$$

($y = \left|g(r)\right|^2$ is the Airy pattern). Using an N-point discrete finite Fourier transform, however, the sample spacing is not in radians but in units of 1/N cycles. If we let ρ = radial frequency in samples, $\rho = \frac{N}{2\pi} w$ and the transform pairs become*

*These relations are approximate, since they do not take into

PSF

$$h(r) = e^{-\frac{1}{2}\left(\frac{r}{\sigma_h}\right)^2} \longleftrightarrow H(\rho) = \left(\frac{N}{2\pi\sigma_H}\right)^2 e^{-\frac{1}{2}\left(\frac{\rho}{\sigma_H}\right)^2} \quad (8)$$

where $\sigma_H \sigma_h = N/2\pi$

Filter

$$g(r) = \frac{2\pi R_1}{N} \cdot \frac{J_1(2\pi R_1 r/N)}{r} \longleftrightarrow G(\rho) = \begin{cases} 1, & \rho < R_1 \\ 0 & \text{otherwise} \end{cases} \quad (9)$$

The width of the Gaussian PSF is

$$W_h = 2\pi\sigma_h^2 = \frac{N^2}{2\pi\sigma_H^2} \quad (10)$$

and the width of the Airy pattern is

$$W_g = \frac{N^2}{\pi R_1^2} \quad (11)$$

Then the "break-even" point is the value of R_1 for which $W_g = W_h$:

$$R_{1e} = \sqrt{2}\ \sigma_H \quad (12)$$

If noise conditions force us to filter at some radius R_1, then the expected improvement in image spread is

$$k = \frac{W_h}{W_g} = \frac{R_1^2}{2\sigma_H^2} \quad (13)$$

2.2 Noise Considerations

In practice, one tries various values of the filter radius, R_1, until the best compromise is obtained between enhancement and noise level. The limits that govern this compromise

---

account the wrap-around and aliasing associated with finite sampled domains. With suitable choice of image size and sampling rate, however, the approximations are close enough.

can be estimated in the following way: The blurring of an image can be considered the result of passing it through a channel whose OTF, $H(\xi,\eta)$ wipes out high-spatial-frequency components of the image. From elementary information theory, the maximum information the blurred image can contain is

$$I_b = B_h \; x_o \; y_o \; k_h \; (bits) \tag{14}$$

where

$$B_b = \frac{\int_{-\infty}^{\infty}\int_{-\infty}^{\infty} |H(\xi,\eta)|^2 \, d\xi \, dy}{|H(0,0)|^2} \tag{15}$$

and

$$K_b = \log_2 (1 + S_b) \tag{16}$$

S_b is the signal-to-noise ratio in the image and x_o and y_o are the dimensions of the image.

Now there are two inputs to the restoration process -- the blurred image and the PSF -- and the information in the restored image can come only from these inputs. If the information in the PSF is $I_h = B_h x_o y_o k_h$ and the information in the restored image is $I_p = B_p x_o y_o k_p$ (where B_h, B_p, k_h, and k_p are defined analogously to equations 15 and 16), then

$$B_p k_p \leq B_h k_h + B_b k_b \tag{17}$$

with equality only if the restoration process takes advantage of all the available information. If we have isoplanaticity, so that b(x, y) and h(x, y) go through identical channels, then $B_b = B_h$; hence we get the following tradeoff between enhancement and noise:

$$\frac{B_p}{B_h} \leq \frac{\log_2(1+S_h) + \log_2(1+S_b)}{\log_2(1+S_b)} \qquad (18)$$

In the case of star pairs, if the stars are of equal magnitude so that $S_h = S_b$, and if we assume that the narrowing of the image is roughly proportional to the widening of the bandwidth, then equation 18 says that we can get, at best, a 2-to-1 improvement in image size if we will accept no degradation of signal-to-noise ratio.

If we return to our Gaussian assumption, we can be more specific. For the Gaussian PSF, $B_n = \pi\sigma_H^2$; for the filter of equation 9, $B_1 = \pi R_1^2$. Then, using the definition of equation 13,

$$k \leq \frac{\ln(1+S_h) + \ln(1+S_b)}{2\ln(1+S_p)} \qquad (19)$$

These results are generally consistent with the experimental results. In particular, for stars with approximately Gaussian images, the actual restoration results closely parallel equation 19, in spite of the rather crude method used for estimating signal-to-noise ratio. Among the representative results singled out in Section 4, the only stars whose results exceed equation 19 are those whose images are clearly non-Gaussian. For the other stars, the results are almost uniformly about 80% of the maximum predicted by equation 19.

3.0 EXPERIMENTAL METHOD

3.1 Data Acquisition

Data were obtained by photographing star pairs at the f/10 focus of the 48-inch telescope at the Range Measurements Laboratory (RML), Patrick Air Force Base. A list of the star pairs observed is given in Table I. The magnitudes range from 2.1 to 6 and the separations from 4.7 to 281 seconds of arc. The exposure time in most cases was 1/125 of a second. No effort was made to photograph star pairs under "good seeing" conditions. Approximately six photographs, spaced about one second apart, were taken of each pair at several elevation angles. The photographs were made using Kodak Tri-X film, which was developed for an ASA of 600 to 800. One frame of each batch of film was exposed to a wedge filter; this image was used to remove the H & D curve from the data. The final result thus indicated intensity instead of density.

For each star pair, four to six best-looking images were selected for digitization. The star images were digitized from the negative by means of the laser image-processing scanner at RML, using a 5-micron spot size (corresponding to a resolution of 0.85 second of arc) and an 8-bit word length. The digitization generated a 128-x-128-point matrix. This was then edited into two 64-x-64-point matrices, each containing one star image. Matrices were written on magnetic tape and sent to FSC for processing. A single tape typically contained several files, each one consisting of three records: a descriptive header record and

records containing the edited images of two stars. Because errors sometimes occurred in editing-out individual star images, files containing the original 128-x-128-point matrices were also included on the tape.

The header record included

- File number
- Sequence number
- Matrix size
- Star identification, right ascension, declination, separation, and visual magnitude (of brighter star)
- Azimuth and elevation at time of exposure
- Time of exposure
- Date
- Duration of exposure
- Coordinates of matrix origin

Each image was written as a set of records, one record for each row of the image matrix.

3.2 Data-Processing Procedures

Each star tape, upon arrival, was given a number, and a table of contents was generated by listing its headers. From the table of contents, the files containing 64-x-64-point arrays were identified. These files were then processed by two programs: the preliminary program and the image-processing program. These will now be described.

The preliminary program reads the files, plots the images contained, and Fourier-transforms the images. In reading the

images, the program converts the fixed-point 8-bit samples into 32-bit floating-point numbers, scaling them so that the sample range of 0 to 255 is converted into data values ranging from 0 to 2.55. The image matrix used in processing is a 64-by-64 array of complex numbers; the program takes the floated sample values and inserts them in the real part of this complex array. Thus, for example, a sample value of 7F (hexadecimal) ends up as the complex number (1.27, 0.). The images are plotted; these plots enable us to judge image quality and to reject any images containing obvious errors. For each pair of images, the program writes a set of output data containing the images and their transforms. The sequence is:

Header (copied from input tape)
First image
Transform of first image
Header
Second image
Transform of second image

The program provides means for specifying the order in which the images are processed. In most cases, the smaller image of the pair was selected first. (This is because the first image is used as the reference PSF in the image-processing program, and it is not reasonable to expect an image to be smaller than the PSF that gave rise to it.)

The image-processing program does the remainder of the data reduction. This consists of the following steps:

Evaluate first image

Evaluate second image

Filter second image

De-convolve

Evaluate resultant image

The image-evaluation, filtering, and de-convolution routines will now be described.

Image Evaluation. These routines compute image centroid, maximum amplitude, signal-to-noise ratios, and four measures of image width. The maximum and centroid computations are trivial and will not be described here. Signal-to-noise ratio is estimated by taking the maximum amplitude as the signal and the standard deviation of the values about the periphery of the matrix as the noise. This is an approximate estimate; it rests on the assumption that the image is narrow and approximately centered in the matrix, so that the values at the edges are mostly noise. These assumptions are usually justified, but occasionally, when the image is unusually big or is badly off-center, the noise estimate goes bad and the measure is worthless. It is usually easy to detect these occurrences, however.

The image-width measures are:

a. Equal-volume area $$W_1 = \frac{\sum_{ij} A(i,j)}{\max(A(i,j))}$$

b. Second-moment area $$W_2 = \frac{\sum_{ij} (i^2+j^2) A(i,j)}{\sum_{ij} A(i,j)}$$

c.

$$W_3 = \frac{\sum_{i,j} (A(i,j))^2}{\left(\sum_{i,j} A(i,j)\right)^2}$$

d. 3-dB area

$$W_4 = \#(\text{pixels} \mid A(i,j) \geq .707 \max(A(i,j))$$

Measures (a) through (c) are computed by a single subroutine. In the case of a restored image, the intensity can sometimes go negative (reference 4); this creates problems for the first three measures and makes their interpretation difficult. To avoid this, the program sums only over the central lobe of the image, stopping at the contour at which the amplitude goes to zero. This contour is found by a search program which tags all pixels belonging to the central lobe. The result of this restriction is that the width estimates for the restored image tend to err by being too optimistic. That is, the numerical measure of image narrowing seems high compared to what we would expect from visually comparing the before-and-after plots. Without this main-lobe restriction, however, the width estimates for the restored images err grossly in the pessimistic direction, and also show little or no consistency. We decided that the main-lobe measures were superior, even with the bias.

Image Filtering. The filter function zeroes out all values in the transform for which the noise is dominant. We assume circular symmetry, since this is the best assumption in the absence of a priori knowledge about the image spectrum. The

filtering function used is shown in Fig. 1.

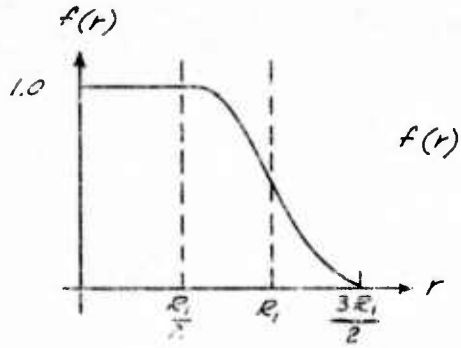

$$f(r) = \begin{cases} 1, & r \le R_1/2 \\ \cos^2\left(\frac{\pi}{2}\frac{r}{R_1} - \frac{\pi}{4}\right), & R_1/2 < r < 3R_1/2 \\ 0, & r \ge 3R_1/2 \end{cases}$$

Fig. 1. Spectrum low-pass filtering function

R_1 is referred to as the truncation radius. In choosing R_1 there is a trade-off between image-width reduction and signal-to-noise ratio, as discussed above (Section 2). The cosine-squared rolloff is used to suppress sidelobes in the restored image.

The filtering program computes the filtering function for a specified value of R_1 and multiplies it by the transform of the image.

De-convolution. Conceptually, the de-convolution program is trivial: it simply divides one Fourier transform by another. (The first image is taken as the reference PSF and its transform (already on the working tape) as the denominator transform; the second image is the one which we attempt to restore and its transform is the numerator.) In practice, the program must be able to detect unreasonable results and try to replace them with reasonable ones. The unreasonable results occur at low S/N levels, where noise drives the denominator transform toward zero. The program attempts to remedy this state of affairs by interpolating from neighboring points, assuming that these are not as badly

affected by noise.

What happens is this: Typically, the S/N ratio near the origin of the Fourier domain is high and there is no trouble. As we move away from the origin, the signal, in both the numerator and the denominator, drops rapidly. Presently, we encounter isolated points where the noise has driven the denominator close to zero. In this region, the program attempts to patch up the denominator by interpolation. As we move into lower and lower S/N regions, the number of such points increases until their density is so great that interpolation does no good. This "hopeless" region is supposed to be eliminated by the image-filtering process described previously. (When the numerator is zero, the program looks no further but immediately sets the quotient to zero at that point.) Thus, the purpose of interpolation is to improve results in the borderline region where only isolated points are seriously corrupted by noise.

If two stars are viewed through a perfectly isoplanatic system, their PSFs will differ only by a constant multiplier, corresponding to their difference in magnitude. Their Fourier transforms will similarly differ, and the deconvolution quotient will be a constant equal to the ratio of the two transforms. Hence this ratio represents the ideal result, and "unreasonable" values are values which differ grossly from this ideal.

In practice, the ratio is not constant. The program approximates the ratio by dividing the integral of the image by that of the reference PSF. (These numbers are already available

since they are the origin values of the respective transforms.) An "unreasonable" quotient point is defined as one whose magnitude is greater than two times this ratio. (This threshold is arbitrarily chosen.)

When an "unreasonable" point is detected, the program does a four-point interpolation of the denominator. That is, if the initial denominator point is d(i,j), then the program computes

$$d'(i,j) = \frac{1}{4}\left[d(i-1,j) + d(i,j-1) + d(i+1,j) + d(i,j+1)\right]$$

and tries again. If the result is still unreasonable, the program throws in four more points --

$$d''(i,j) = \frac{1}{2}d'(i,j) + \frac{1}{8}\left[d(i-1,j-1) + d(i-1,j+1) + d(i+1,j-1) + d(i+1,j+1)\right]$$

and tries a third time. If the quotient is still unacceptable, then its magnitude is forced to the ideal value and the point is flagged for further attention.

After the process is complete, the flagged values are examined. A four-point interpolation, similar to that described above for the denominator, is attempted, but only if the four reference points are unflagged. (This technique is not as successful as might be expected, because unsatisfactory points tend to cluster.)

4.0 EXPERIMENTAL RESULTS

The results obtained for all star-pairs processed are presented in Tables 2 through 10 at the end of this section. Following these tables, plots for selected pairs are shown in Figures 2 through 20. These plots are also referenced at the corresponding locations in the tables. Most of the table entries are self-explanatory. "Sequence No." refers to the tape and file numbers which identify the image. In most cases, the smaller image was used as the PSF, but occasionally the images were interchanged, particularly if they were approximately the same size, to see whether better results were obtained that way. "Improvement" is given as the ratio of width before processing to width after processing: thus, the larger the ratio the better the improvement.

The descriptions under "Appearance" are subjective evaluations of restored-image quality as judged from looking at the 3-D plots. They are intended to supplement, and in some cases to correct, the numerical entries. As we mentioned in the preceding section, the numerical results of image evaluation are not always consistent. Although descriptions such as "very good" and "fair" are necessarily vague, they are at least not misleading. In addition, their significance is clarified by the 3-D plots supplied for selected stars.

Restoration with any given star pair was largely a cut-and-try procedure using different values of the filter radius, R1. Where practical, we tried to find a value giving the best

trade-off between image size and noise level. Because available computer time was limited, we were not always able to try as many values as might be desired. In some cases, we quickly found that no satisfactory trade-off was to be found and the search was abandoned.

Tables 9 and 10 present a selected subset of the processing results. (The rule for selection is to choose the result for which the estimated signal-to-noise ratio in the restored image is closest to 30 dB.) Inspection of these tables shows the following:

1. Width enhancement, using the equivalent-area measure (W1) averages 1.71. (A ratio of 1.00 indicates no improvement at all.)

2. There is no correlation between enhancement and separation.

3. There is no correlation between enhancement and elevation angle.

Examination of the star data reveals two significant facts. First, nearly all star images look Gaussian. This is inconsistent with what we had been led to expect: images degraded by turbulence were supposed to be "broken up" and "torn apart." Image tear was never seen, however. The images in Figures 2 and 3 are representative of what was obtained most of the time. In fact, most of the images of most of the stars looked alike. To test this, we tried restoring two unrelated images. This experiment was run twice, first with two images from star-pair 48

taken some seconds apart; second with two images taken two months apart. The results, shown in Table 11 and Figures 18 and 19, are roughly comparable to the average enhancements obtained in the main experiment. Finally, enhancement was attempted with a computer-generated Gaussian pulse, tailored to fit the star image. The result (Fig. 20 and Table 11) was slightly better than the average, and distinctly better than what we had achieved using the star's own companion image (Fig. 5).

If the images are Gaussian, then it should be possible to check the results in Table 9 against equation 19. In spite of the rather crude method used for estimating the signal-to-noise ratio, the results are generally consistent. The exceptions are stars whose images are visibly non-Gaussian, notably the 1-msec exposure of Star 40.

The other unexpected result is that the images are not of equal size. The brighter star always has a wider image, and the difference in width is roughly proportional to the difference in magnitude. In a linear, isoplanatic system, the star images can be expected to differ by noise and by a multiplicative constant. Neither of these differences can cause the differences in image size seen here.

One possible explanation for the Gaussian shape is blurring resulting from too long an exposure. (See, for example, references 3 and 4.) This possibility is suggested by the extraordinarily good results obtained with the one 1-msec exposure investigated. Star 40, sequence #7/7 and 7/8, shown in Table 5

and in Figs. 6, 7, 8, and 9, yielded the best overall enhancement of all the images processed. The evidence of a single image cannot be conclusive, of course, but it is suggestive, especially since the images come closer to showing image tear than any others.

The unequal size is most likely the result of non-linearities in recording the received images. Either the exposure was so weak that the images fell at the non-linear "toe" of the H & D curve for Tri-X, or else the logarithmic H & D curve itself was improperly removed. Another possibility is that light scatter occurred within the relatively thick emulsion of the Tri-X film. (Scatter would also tend to make torn images look Gaussian.) This would suggest that the exposure was too strong, however, rather than too weak. Calculations based on visual magnitude, aperture size, etc., have not been conclusive, but the images, as seen on the film, do not look dense enough for scatter to be likely.

TABLE 1 STAR-PAIR DATA RECEIVED FROM RML

I.D. No.	SEPA-RATION	RIGHT ASCENSION	DECLI-NATION	MAGNI-TUDES	TAPE No.	DATE	TIME	AZI-MUTH	ELEVA-TION
24	3.9 sec	15.324	10.420	3.0 ,4.0	7	4/26/73	12:50	143.	69.
					9	4/26/73	1:07	154.	71.
27	6.3	3.416	27.450	4.1 ,5.0	8	4/26/73	12:49	50.	75.
32	13.7	16.025	0.	2.0, 6.0	8	4/26/73	1:01	158.	39.
					9	4/26/73	1:16	163.	40.
40	4.7	12.391	-.004	3.0, 3.0	2	2/4/73	1:52	*	*
					7	4/26/73	12:42	228.	50.
43	19.8	12.537	38.46	3.2, 5.7	4	4/2/73	2:03	305.	69.
47	284.1	13.130	38.767	5.5, 5.9	5	4/2/73	2:33	303.	66
48	14.5	13.219	55.110	2.1, 4.2	1	2/4/73	1:53	*	*
					6	4/2/73	3:16	327.	54.

* These data not supplied

TABLE 2. SUMMARY OF RESULTS FOR STAR-PAIR #24

Right Ascension 15.324 Declination 10.420
Magnitude 3.0, 4.0 Separation 3.9 sec of arc

IMAGE SEQ. No.	PSF SEQ. No.	EXPO-SURE (ms)	AZ (deg)	EL (deg)	IMAGE S/N (dB)	PSF S/N (dB)	FILTER R1	IMPROVEMENT W1	W2	W3	W4	RESULT S/N (dB)	APPEARANCE Width	S/N (dB)	NOTES
7/10	7/9	8	143.	69.	28.7	13.4	6.	2.79	3.06	2.06	3.22	13.4	bad	bad	
7/12	7/11	8	143.	69.	47.8	45.1	10.	1.28	1.25	.39	1.16	38.0	good	exc.	
9/5	9/6	8	154.	71.	20.2	32.7	6.	3.34	4.85	1.35	1.08	16.3	bad	bad	
9/8	9/7	8	154.	71.	48.2	23.5	12.	.60	.69	.134	.50	26.8	good	good	

Notes:

TABLE 3. SUMMARY OF RESULTS FOR STAR-PAIR #27

Right Ascension 3.416 Declination 27.450
Magnitude 4.1, 5.0 Separation 6.3 sec of arc

IMAGE SEQ. No.	PSF SEQ. No.	EXPO-SURE (ms)	AZ (deg)	EL (deg)	IMAGE S/N (dB)	PSF S/N (dB)	FILTER R1	IMPROVEMENT W1	W2	W3	W4	RESULT S/N (dB)	APPEARANCE Width	APPEARANCE S/N (dB)	NOTES
8/8	8/7	8	50.	75.	45.9	48.2	9.	.89	3.05	5.12	.10	43.8	exc.	exc.	
8/8	8/7	8	50.	75.	45.9	48.2	12.	1.55	5.77	9.03	.25	41.0	exc.	exc.	
8/8	8/7	8	50.	75.	45.9	48.2	16.	1.89	6.29	10.95	.25	36.0	v.g.	v.g.	

Notes:

TABLE 4. SUMMARY OF RESULTS FOR STAR-PAIR #32

Right Ascension 16.025 Declination 0.
Magnitude 2.0, 6.0 Separation 13.7 sec of arc

IMAGE SEQ. No.	PSF SEQ. No.	EXPO-SURE (ms)	AZ (deg)	EL (deg)	IMAGE S/N (dB)	PSF S/N (dB)	FILTER R1	IMPROVEMENT W1	W2	W3	W4	RESULT S/N (dB)	APPEARANCE Width	S/N (dB)	NOTES
8/10	8/9	8	158.	39.	28.0	36.8	6.	3.82	6.67	1.69	1.3	15.3	bad	bad	1
8/9	8/10	8	158.	39.	36.8	28.0	9.	3.41	2.92	2.21	16.5	17.8	bad	bad	2
8/12	8/11	8	158.	39.	48.2	48.2	6.	.095	.069	.016	.035	37.3	fair	good	2
8/11	8/12	8	158.	39.	48.2	48.2	9.	.84	.99	.93	.5	48.2	exc.	exc.	1
8/11	8/12	8	158.	39.	48.2	48.2	24.	1.04	1.07	.79	1.56	42.9	fair	exc.	1,3
9/10	9/9	8	163.	40.	41.3	48.2	18.	3.38	9.0	4.57	1.0	32.1	good	v.g.	4
9/12	9/11	8	163.	40.	25.2	35.9	9.	4.01	7.78	2.36	.5	16.1	bad	bad	

Notes:
1. Smaller image used as PSF.
2. Larger image used as PSF.
3. Restored image broken up.
4. Very many side lobes

TABLE 5 . SUMMARY OF RESULTS FOR STAR-PAIR #40

Right Ascension 12.391 Declination -.004
Magnitude 3.0, 3.0 Separation 4.7 sec of arc

IMAGE SEQ. No.	PSF SEQ. No.	EXPO-SURE (ms)	AZ (deg)	EL (deg)	IMAGE S/N (dB)	PSF S/N (dB)	FILTER R1	IMPROVEMENT W1	W2	W3	W4	RESULT S/N (dB)	APPEARANCE Width	S/N (dB)	NOTES
2/13b	2/13a	8	-	-	27.5	29.3	5.	2.94	3.22	1.08	1.87	15.7	fair	fair	1,5
2/14b	2/14a	8	-	-	46.5	45.4	6.	.66	1.0	.52	.32	9.8	fair	fair	1
2/15b	2/15a	8	-	-	47.0	46.6	6.	.84	.89	.28	.75	15.9	bad	bad	1
2/16b	2/16a	8	-	-	28.2	30.4	6.	2.10	2.45	.94	4.11	11.8	bad	bad	1
2/17b	2/17a	8	-	-	39.7	38.6	6.	1.35	1.94	.75	.27	23.6	good	good	1
7/6	7/5	2	228.	50.	48.2	48.2	8.	1.01	.795	.193	.35	25.1	fair	good	
7/5	7/6	2	228.	50.	48.2	48.2	10.	1.05	.863	.243	.76	21.0	fair	good	2
7/8	7/7	1	228.	50.	40.0	35.7	9.	1.73	5.81	2.41	.38	29.5	good	v.g.	2
7/7	7/8	1	228.	50.	35.7	40.0	9.	3.57	12.6	7.16	.035	34.0	exc.	exc.	3
7/8	7/7	1	228.	50.	40.0	35.7	12.	2.14	6.63	2.58	.6	29.9	v.g.	v.g.	2
7/7	7/8	1	228.	50.	35.7	40.0	12.	4.62	14.8	8.1	.125	30.0	v.g.	v.g.	3
7/7	*	1	228.	50.	35.7	*	12.	.63	1.15	1.35	.05	38.1	exc.	exc.	4,6

Notes:
1. Az and el data not supplied for these images
2. Larger image used as PSF
3. Smaller image used as PSF
4. Image filtered only, not restored
5. These images are illustrated in Figs. 2, 3, 4, and 5
6. These images are illustrated in Figs. 6, 7, 8, and 9

TABLE 6. SUMMARY OF RESULTS FOR STAR-PAIR #43

Right Ascension 12.537 **Declination** 38.46
Magnitude 3.2, 5.7 **Separation** 19.8 sec of arc

IMAGE SEQ. No.	PSF SEQ. No.	EXPO-SURE (ms)	AZ (deg)	EL (deg)	IMAGE S/N (dB)	PSF S/N (dB)	FILTER R1	IMPROVEMENT W1	W2	W3	W4	RESULT S/N (dB)	APPEARANCE Width	S/N (dB)	NOTES
4/8	4/7	8	305.	69.	48.2	48.2	6.	.814	.979	1.045	.47	41.8	exc.	exc.	
4/8	4/	8	305.	69.	48.2	48.2	12.	1.47	1.70	.768	2.33	41.9	fair	exc.	1,3
4/8	4/7	8	305.	69.	48.2	48.2	∞	3.22	2.98	.488	7.0	29.4	bad	fair	
4/10	4/9	8	305.	69.	48.2	48.2	9.	.915	.978	1.09	.43	39.7	v.g.	exc.	
4/10	4/9	8	305.	69.	48.2	48.2	15.	1.33	1.40	.692	1.5	27.9	good	good	
4/10	4/9	8	305.	69.	48.2	48.2	24.	3.62	3.79	.493	9.0	25.8	bad	fair	2
4/10	4/9	8	305.	69.	48.2	48.2	∞	3.69	3.27	.420	4.5	25.3	bad	fair	2
4/12	4/11	8	305.	69.	48.2	48.2	9.	1.0	1.12	1.05	.5	25.2	v.g.	exc.	
4/12	4/11	8	305.	69.	48.2	48.2	18.	1.52	1.03	.30	2.75	25.4	poor	good	
4/12	4/11	8	305.	69.	48.2	48.2	34.	3.57	2.46	.365	11.0	28.0	bad	fair	
4/16	4/15	8	305.	69.	48.2	48.2	9.	.795	1.01	1.10	5.6	38.4	exc.	exc.	
4/16	4/15	8	305.	69.	48.2	48.2	18.	1.84	1.91	.606	2.5	28.8	fair	good	
4/16	4/15	8	305.	69.	48.2	48.2	∞	3.15	2.93	.628	2.5	29.1	bad	fair	

Notes:
1. Some breakup in restored image
2. Restored image badly broken up
3. These images are illustrated in Figs. 10, 11, 12, and 13.

TABLE 7. SUMMARY OF RESULTS FOR STAR-PAIR #47

Right Ascension 13.130 Declination 38.767
Magnitude 5.5, 5.9 Separation 284.1 sec of arc

IMAGE SEQ. No.	PSF SEQ. No.	EXPO-SURE (ms)	AZ (deg)	EL (deg)	IMAGE S/N (dB)	PSF S/N (dB)	FILTER R1	IMPROVEMENT W1	W2	W3	W4	RESULT S/N (dB)	APPEARANCE Width	S/N (dB)	NOTES
5/7	5/6	8	303.	66.	42.2	39.5	6.	1.51	1.73	3.63	1.37	26.4	good	exc.	
5/7	5/6	8	303.	66.	42.2	39.5	9.	2.15	1.80	2.28	12.5	20.61	bad	fair	
5/6	5/7	8	303.	66.	39.5	42.2	6.	1.09	1.59	1.16	1.12	22.7	fair	fair	
5/9	5/8	8	303.	66.	46.0	39.1	6.	1.86	1.74	1.56	1.94	13.3	poor	good	
5/9	5/8	8	303.	66.	46.0	39.1	9.	2.36	1.84	1.11	4.42	13.8	poor	fair	

Notes:

TABLE 8 . SUMMARY OF RESULTS FOR STAR-PAIR #48

Right Ascension 13.219 Declination 55.110
Magnitude 2.1, 4.2 Separation 14.5 sec of arc

IMAGE SEQ. No.	PSF SEQ. No.	EXPO-SURE (ms)	AZ (deg)	EL (deg)	IMAGE S/N (dB)	PSF S/N (dB)	FILTER R1	IMPROVEMENT W1	W2	W3	W4	RESULT S/N (dB)	APPEARANCE Width	S/N (dB)	NOTES
1/2	1/1	8	-	-	42.0	38.5	3.0	1.66	2.02	3.98	1.53	17.8	exc.	exc.	1,3
1/2	1/1	8	-	-	42.0	38.5	4.5	1.70	2.26	4.59	1.26	18.9	exc.	exc.	1
1/2	1/1	8	-	-	42.0	38.5	6.0	2.27	3.44	5.75	1.24	17.9	v.g.	exc.	1
1/2		8	-	-	42.0		6.0	1.07	1.13	1.60	1.11	47.4	exc.	exc.	1,2,3
1/6	1/5	8	-	-	48.2	48.1	12.	1.25	1.30	1.16	1.43	35.6	good	exc.	1
1/6	1/5	8	-	-	48.2	48.1	15.	1.51	1.36	.74	3.54	32.6	good	good	1
1/8	1/7	8	-	-	48.2	47.7	10.	1.27	1.12	.38	1.85	23.9	v.g.	good	1
1/8	1/7	8	-	-	48.2	47.7	13.	1.71	1.30	.48	5.29	23.8	fair	fair	1
1/10	1/9	8	-	-	48.2	45.6	9.	1.22	1.38	1.38	.98	37.8	v.g.	exc.	1
1/10	1/9	8	-	-	48.2	45.6	12.	1.46	1.29	.43	2.75	23.8	fair	v.g.	1
1/12	1/11	8	-	-	48.2	44.0	6.	1.26	1.41	1.12	.924	29.3	exc.	exc.	1
1/12	1/11	8	-	-	48.2	44.0	9.	1.67	1.64	1.21	2.5	22.0	good	fair	1
6/7	6/6	8	327.	54.	35.7	37.0	6.	2.48	2.03	1.10	5.95	14.7	bad	bad	
6/9	6/8	8	327.	54.	36.7	38.7	6.	2.71	2.3	.81	10.7	12.0	bad	bad	
6/11	6/10	8	327.	54.	34.1	38.0	6.	3.35	2.24	.89	3.55	13.8	fair	poor	
6/13	6/12	8	327.	54.	30.3	38.6	6.	3.52	2.83	1.08	9.32	11.6	poor	bad	
6/12	6/13	8	327.	54.	38.6	30.3	6.	1.61	1.85	.77	1.44	15.6	poor	poor	
6/15	6/14	8	327.	54.	36.0	25.1	6.	2.33	2.33	1.19	3.15	14.3	bad	bad	

Notes: 1. Az, el data not supplied for these images
2. Image filtered only, not restored
3. These images are illustrated in Figs. 14, 15, 16, and 17

TABLE 9 REPRESENTATIVE RESULTS IN ORDER OF SEPARATION

SEPARATION (sec)	No.	DATE	TIME	S/N RATIO (dB)		MAGNITUDE	EXPOSURE (ms)	ENHANCEMENT				RESULT S/N (dB)	QUALITY
				IMAGE	PSF			W1	W2	W3	W4		
4.7	24	4/26/73	12:50	47.8	45.1	3.0,4.0	8	1.28	1.25	.39	1.16	38.0	good
4.7	24	4/26/73	1:07	48.2	23.5	3.0,4.0	8	.60	.69	.134	0.50	26.8	good
4.7	40	2/4/73	1:52	39.7	38.6	3.0,3.0	8	1.35	1.94	.75	0.27	23.6	good
4.7	40	4/26/73	12:42	35.7	40.0	3.0,3.0	1	4.62	14.8	8.1	0.13	30.0	v. good
6.3	27	4/26/73	12:49	45.9	48.2	4.1,5.0	8	1.89	6.29	10.95	0.25	36.0	v. good
13.7	32	4/26/73	1:01	48.2	48.2	2.0,6.0	8	.095	.069	.016	0.04	37.3	fair
13.7	32	4/26/73	1:16	41.3	48.2	2.0,6.0	8	3.38	9.0	4.57	1.00	32.1	good
14.7	48	2/4/73	1:53	48.2	44.0	2.1,4.2	8	1.26	1.41	1.12	0.92	29.3	exc.
14.7	48	4/2/73	3:16	38.6	30.3	2.1,4.2	8	1.61	1.85	.77	1.44	15.6	poor
19.8	43	4/2/73	2:03	48.2	48.2	3.2,5.7	8	1.33	1.40	.692	1.5	27.9	good
284.1	47	4/2/73	2:33	48.2	39.5	5.5,5.9	8	1.51	1.73	3.03	1.37	26.4	good

Note: Results selected for the S/N nearest 30 dB. When the choice was not clear-cut, the result with the best image quality was selected.

TABLE 10 REPRESENTATIVE RESULTS IN ORDER OF ELEVATION ANGLE

ELEVATION	AZIMUTH	No.	DATE	TIME	SEPARATION (sec)	MAGNITUDE	EXPOSURE (ms)	ENHANCEMENT W1	W2	W3	W4	RESULT S/N (dB)	QUALITY
75	50	27	4/26/73	12:49	6.3	4.1,5.0	8	1.89	6.29	10.95	.25	36.3	v. good
71	154	24	4/26/73	1:07	4.7	3.0,4.0	8	0.60	0.69	.134	.5	26.8	good
69	305	43	4/2/73	2:03	19.8	3.2,5.7	8	1.33	1.40	.692	1.5	27.9	good
69	143	24	4/26/73	12:50	4.7	3.0,4.0	8	1.28	1.25	.39	1.16	38.4	good
66	303	47	4/2/73	2:33	284.1	5.5,5.9	8	1.51	1.73	3.03	1.37	26.4	good
54	327	48	4/2/73	3:16	14.7	2.1,4.2	8	1.61	1.85	.77	1.44	15.6	poor
50	228	40	4/26/73	12:42	4.7	3.0,3.0	1	4.62	14.8	8.1	.125	30.0	v. good
40	163	32	4/26/73	1:16	13.7	2.0,6.0	8	3.38	9.0	4.57	1.0	32.2	good
39	158	32	4/26/73	1:01	13.7	2.0,6.0	8	0.10	.069	.016	.035	37.7	fair

Note: Results selected for the S/N nearest 30 dB. When the choice was not clear-cut, the result with the best image quality was selected.

TABLE 11. SUMMARY OF RESULTS OF SPECIAL EXPERIMENTS

IMAGE SEQ. No.	PSF SEQ. No.	EXPO-SURE (ms)	AZ (deg)	EL (deg)	IMAGE S/N (dB)	PSF S/N (dB)	FILTER R1	IMPROVEMENT W1	W2	W3	W4	RESULT S/N (dB)	APPEARANCE Width	S/N (dB)	NOTES
1/1	1/8	8	-	-	38.5	∞	6.0	2.33	3.82	1.49	1.21	25.47	exc.	v.g.	1,2
5/7	1/1	8	-	-	43.4	38.5	6.0	1.53	1.94	3.37	1.05	14.92	v.g.	exc.	3,4
1/1	-	8	-	-	38.5	∞	6.0	4.24	7.33	2.96	1.92	29.64	exc.	v.g.	5,6

Notes:
1. Two images from star-pair 48, photographed 5 sec. apart
2. This result is illustrated in Fig. 18
3. Images from star-pairs 47 and 48, photographed 2 months apart
4. This result is illustrated in Fig. 19
5. Image from star-pair 48, deconvolved with Gaussian pulse ($\sigma = 5$)
6. This result is illustrated in Fig. 20

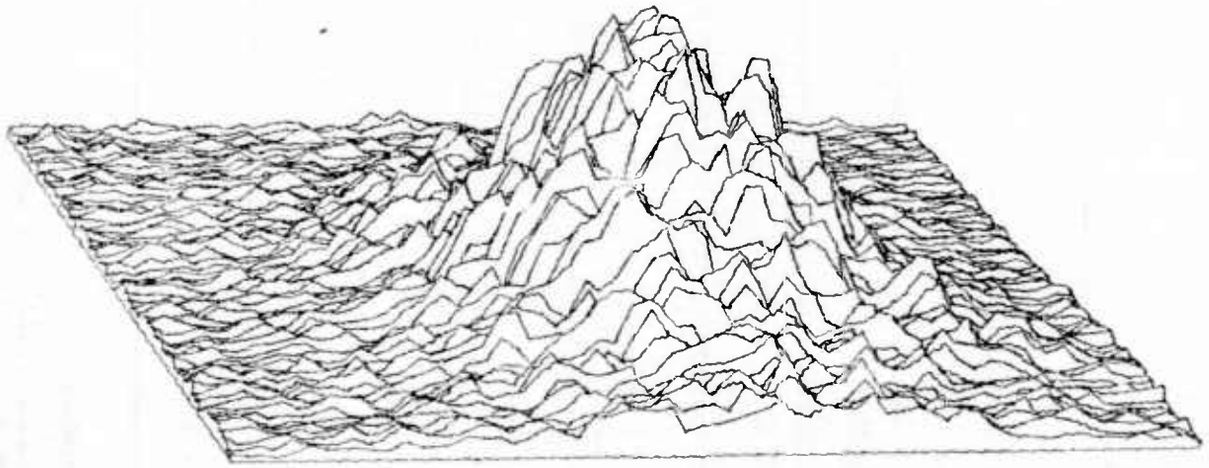

Figure 2. Star 40, Sequence No. 2/13a

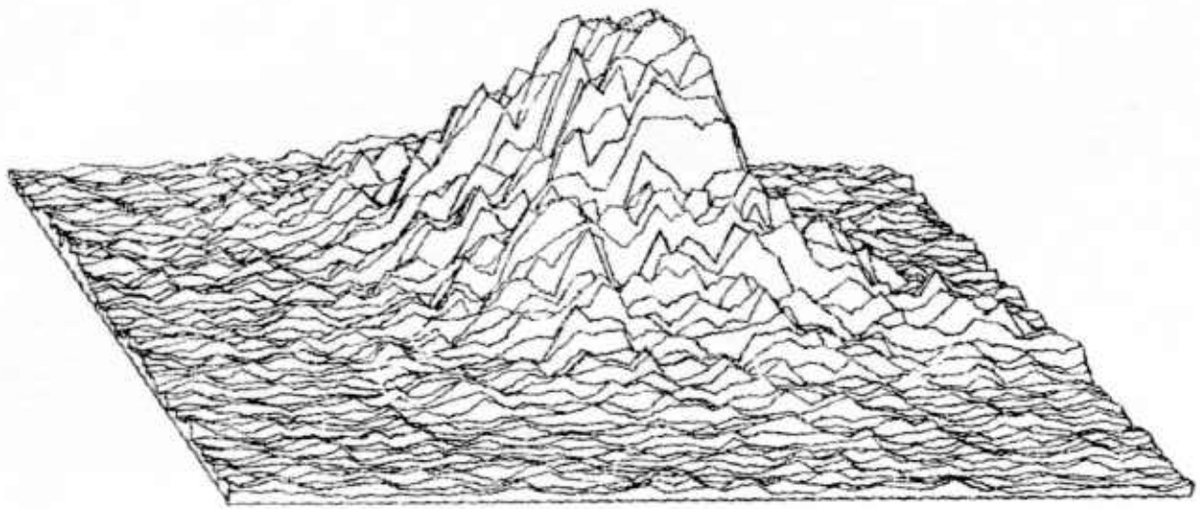

Figure 3. Star 40, Sequence No. 2/13b

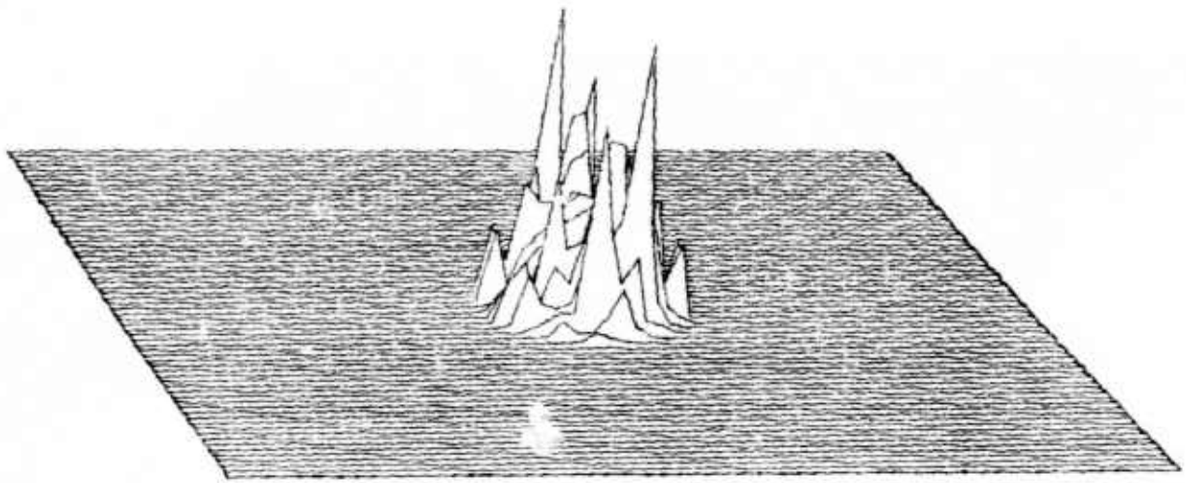

Figure 4. Star 40, Sequence No. 2/13a and b - Deconvolution Quotient

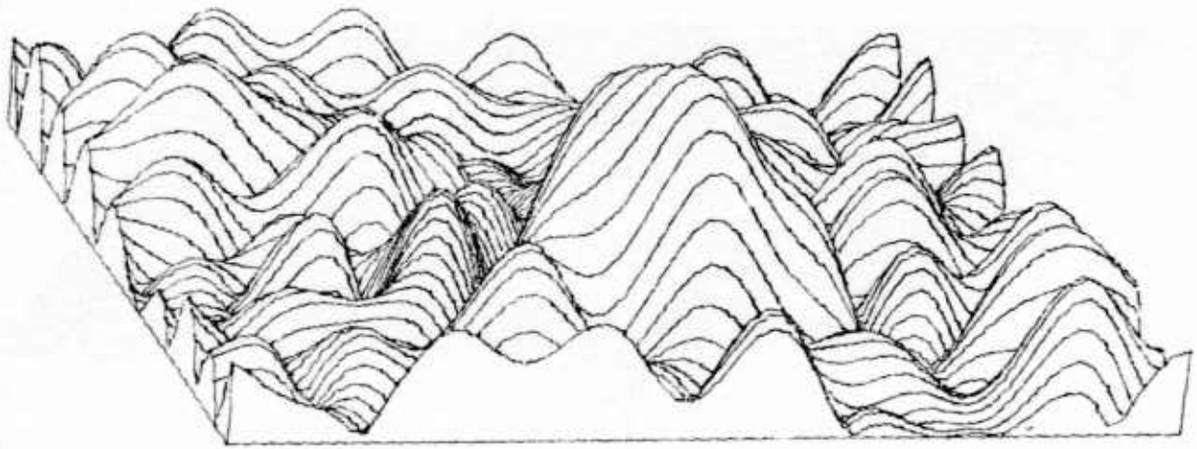

Figure 5. Star 40, Sequence No. 2/13a and b - Restored Image

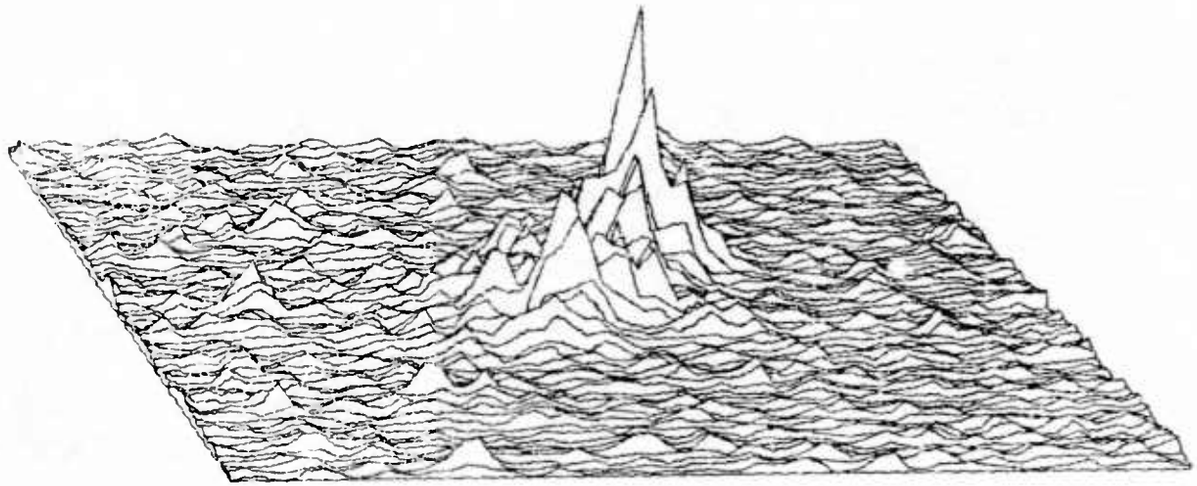

Figure 6. Star 40, Sequence No. 7/7

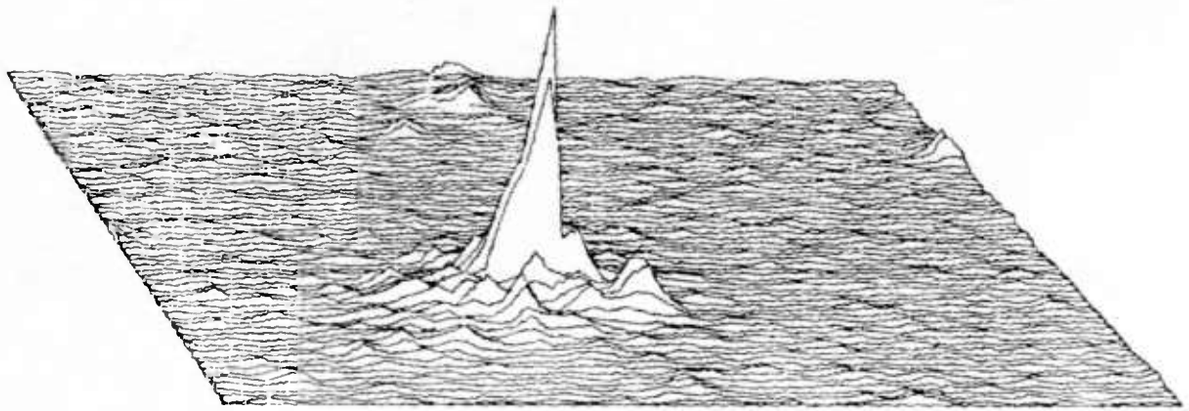

Figure 7. Star 40, Sequence No. 7/8

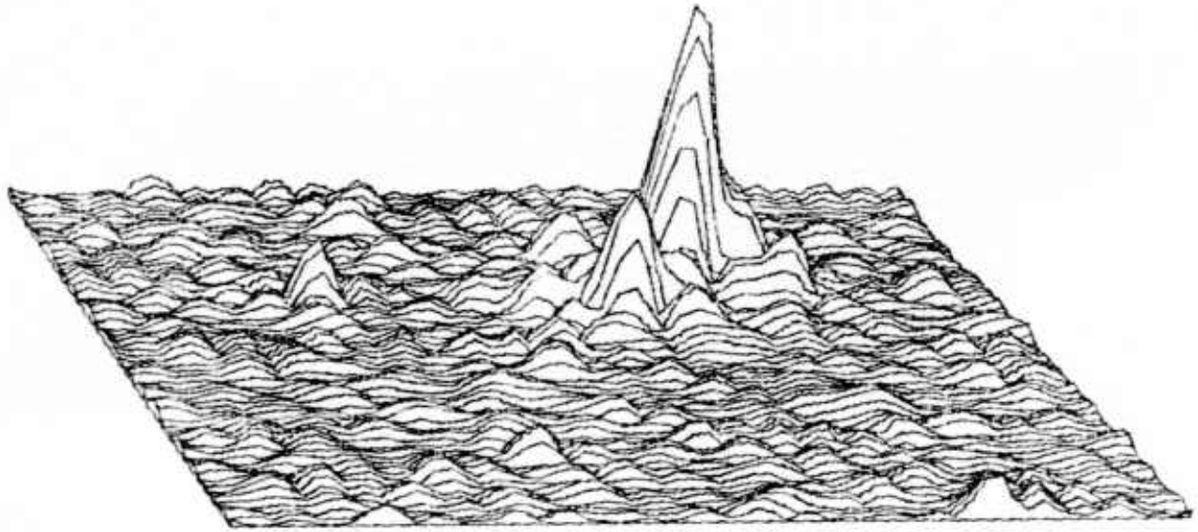

Figure 8. Star 40, Sequence No. 7/7 and 7/8 - Restored Image

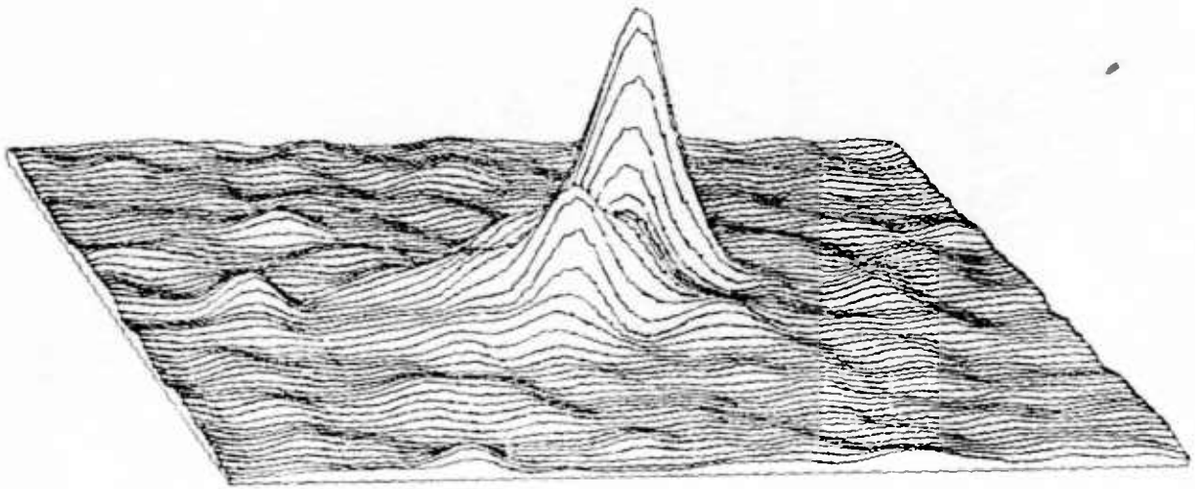

Figure 9. Star 40, Sequence No. 7/7 - Filtered Only

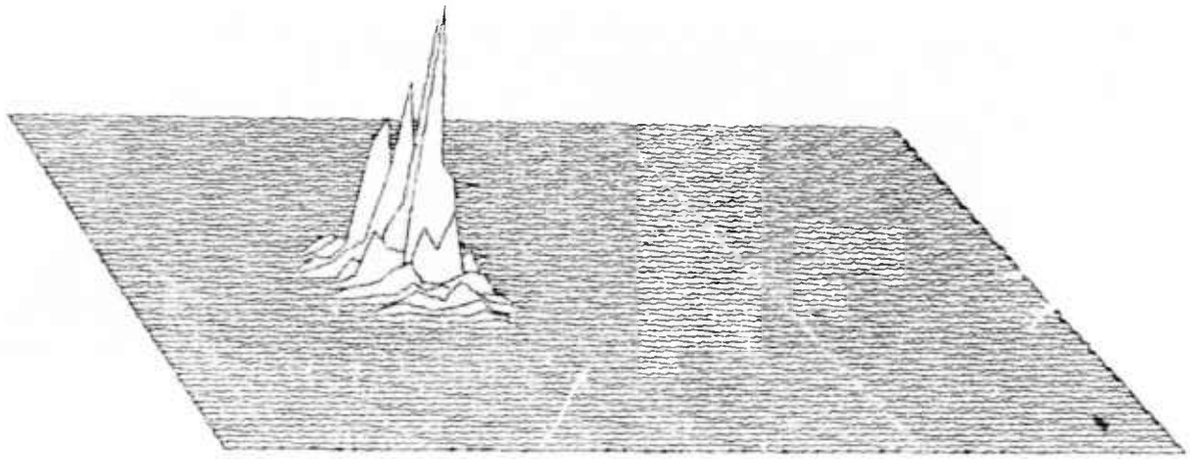

Figure 10. Star 43, Sequence No. 4/7

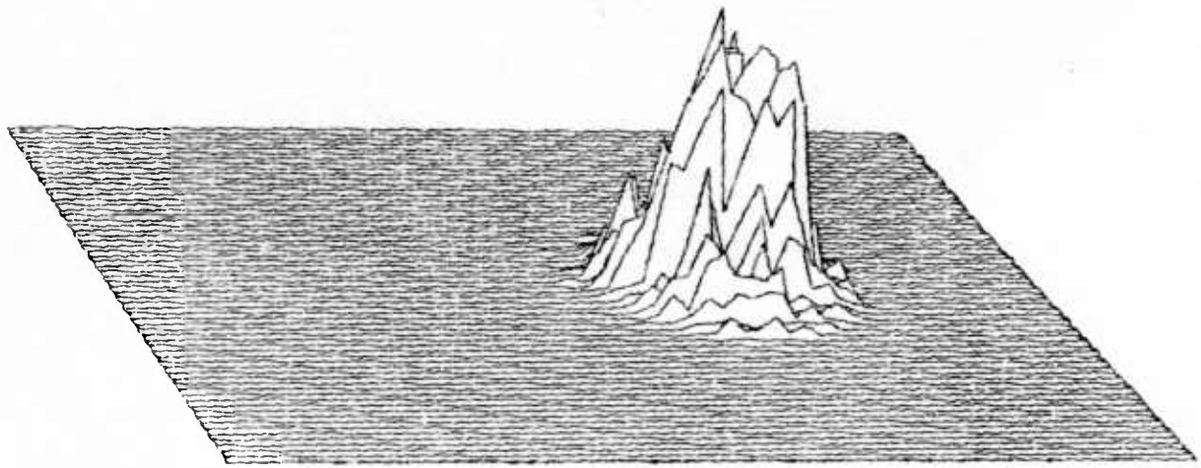

Figure 11. Star 43, Sequence No. 4/8

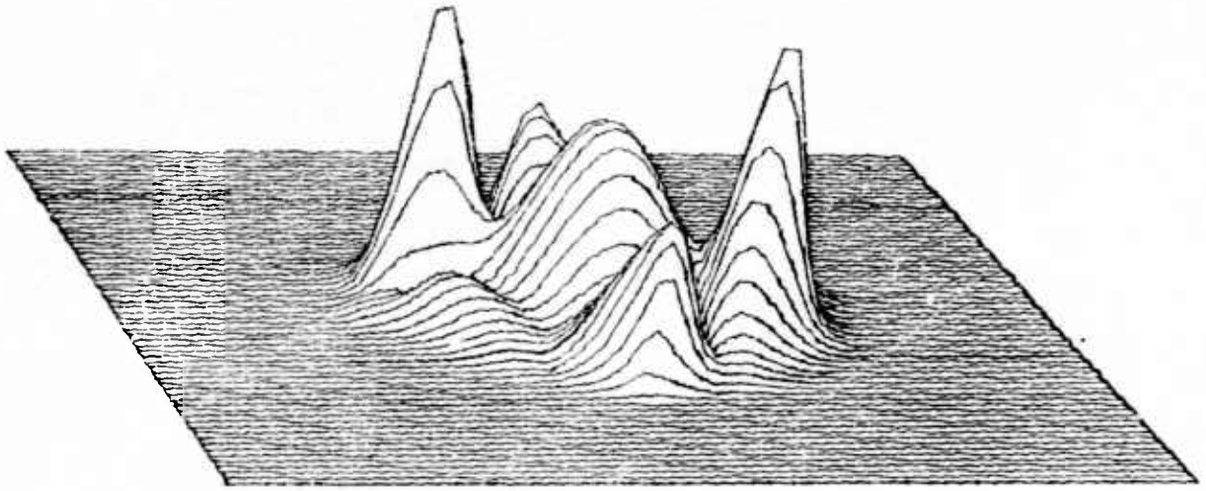

Figure 12. Star 43, Sequence No. 4/7 and 4/8 - Deconvolution Quotient

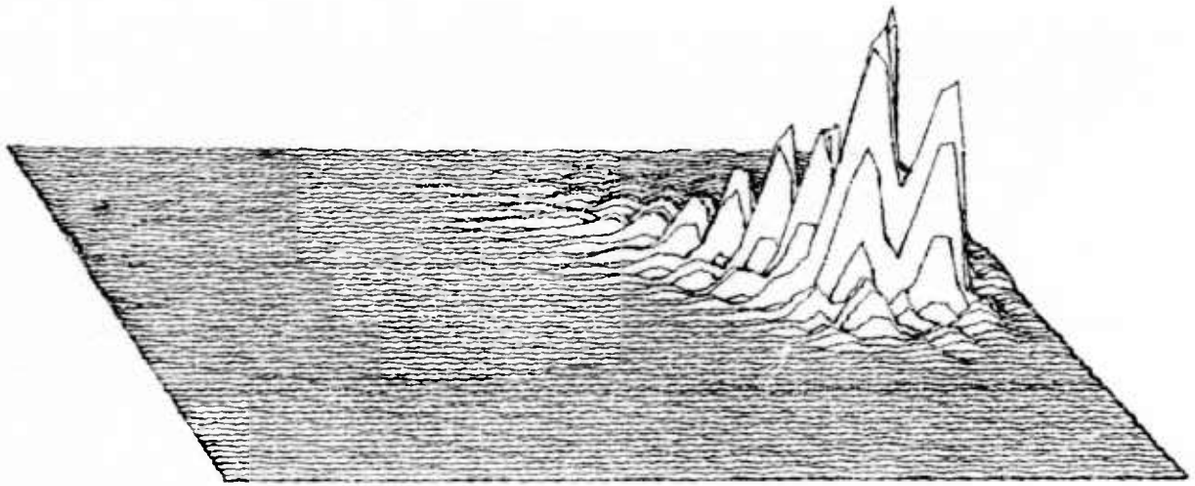

Figure 13. Star 43, Sequence No. 4/7 and 4/8 - Restored Image

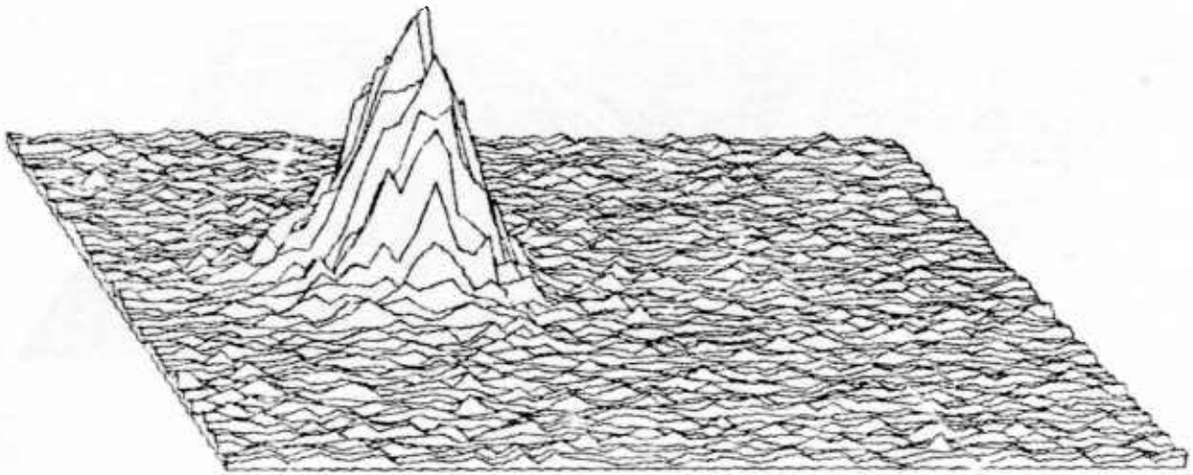

Figure 14. Star 48, Sequence No. 1/1

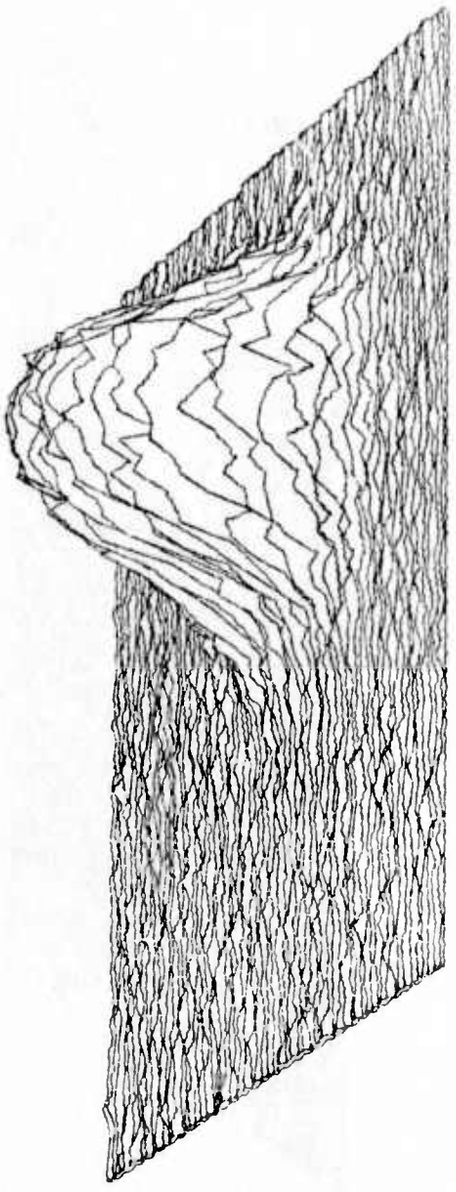

Figure 15. Star 48, Sequence No. 1/2

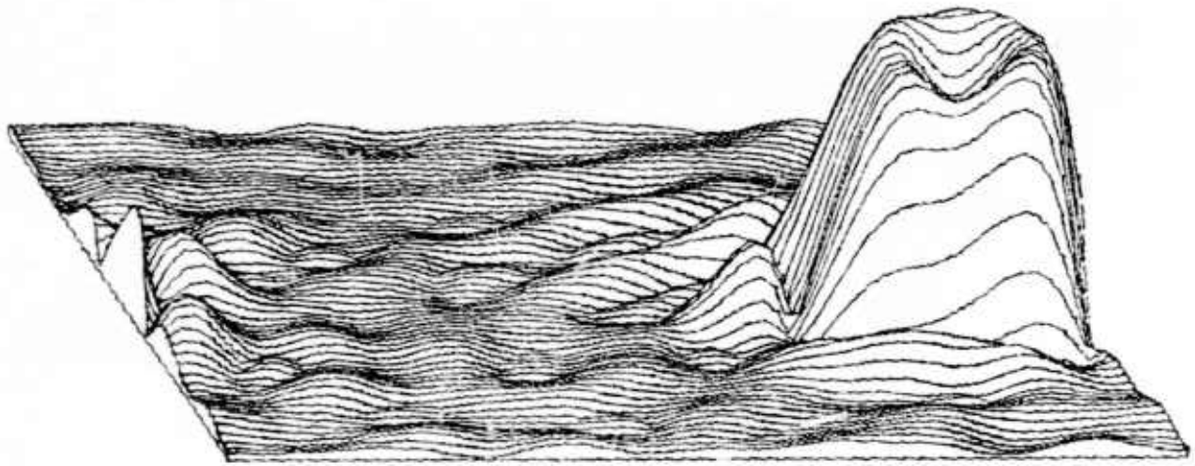

Figure 16. Star 48, Sequence No. 1/1 and 1/2 - Restored Image

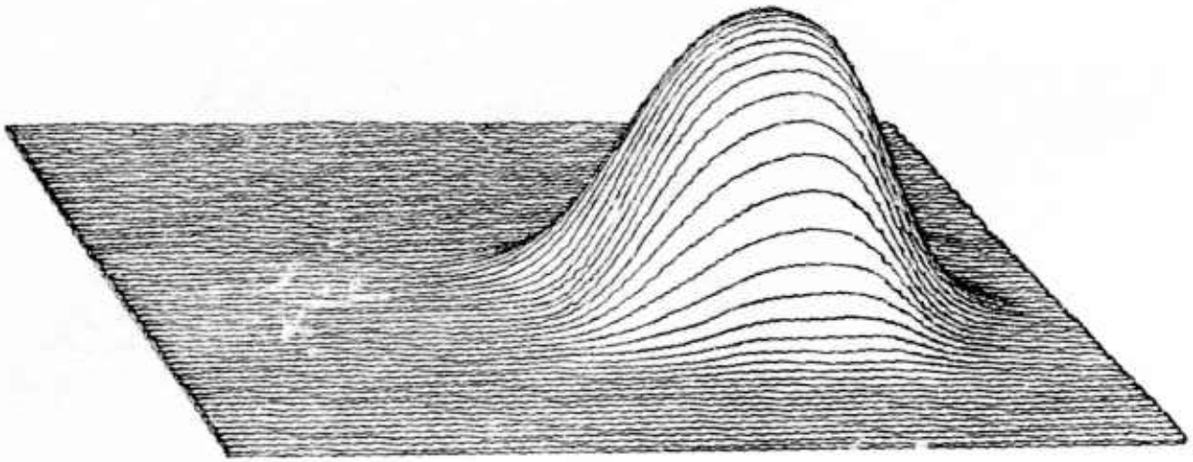

Figure 17. Star 48, Sequence No. 1/2 - Filtered Only

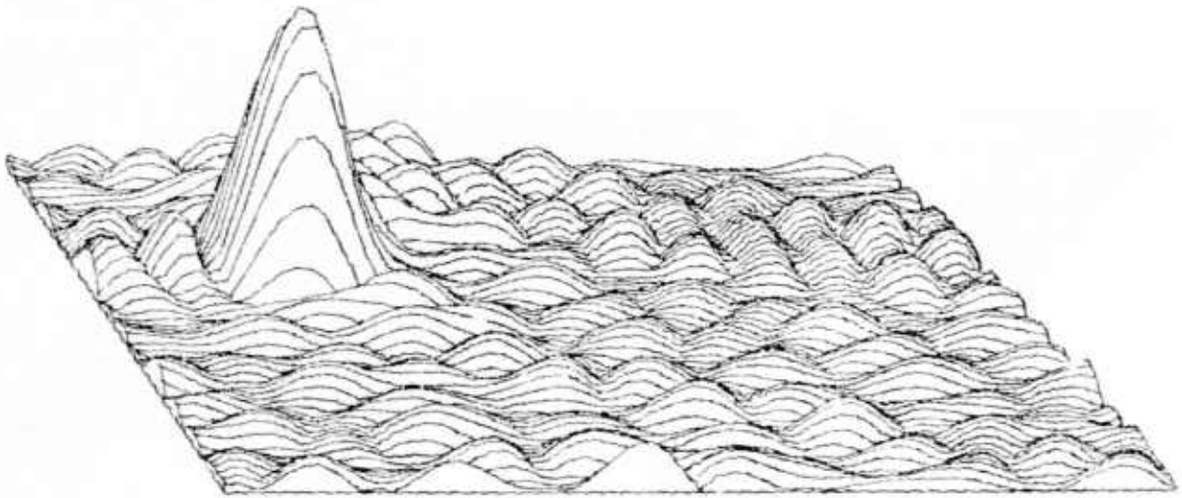

Figure 18. Star 48, Sequence No. 1/1 and 1/8 - Restored Image

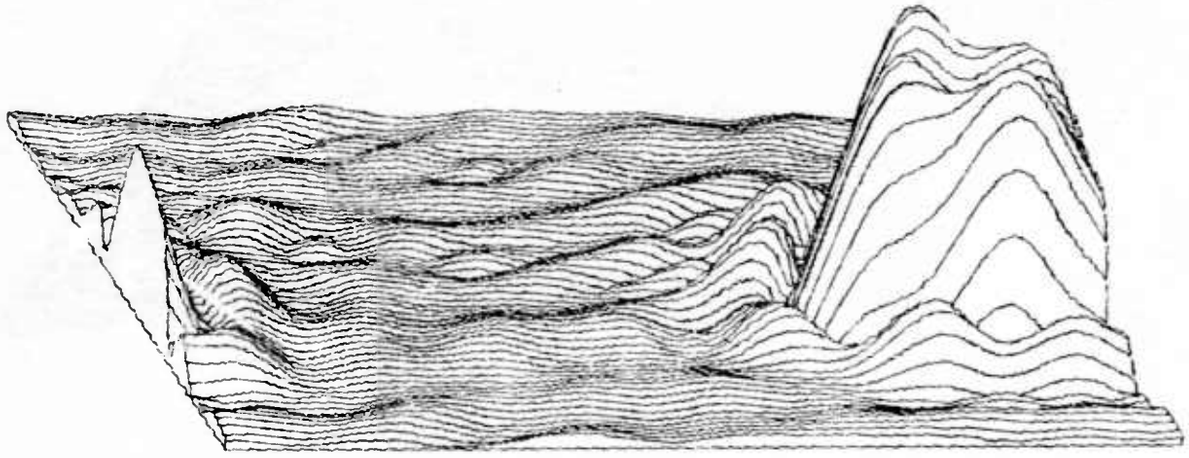

Figure 19. Star 47, Sequence No. 5/7 and Star 48, Sequence No. 1/1 - Restored Image

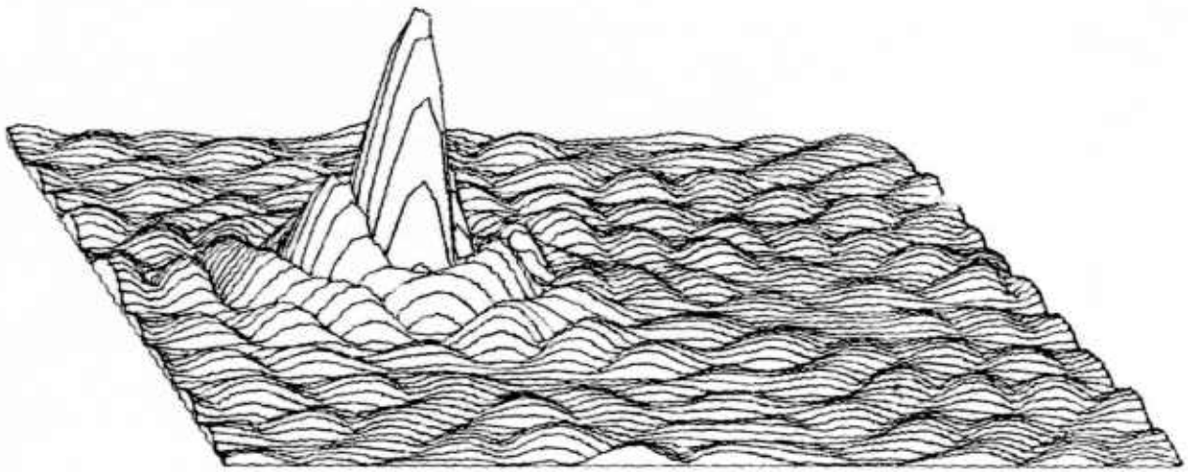

Figure 20. Star 48, Sequence No. 1/1 Deconvolved with Gaussian Pulse - Restored Image

5.0 CONCLUSIONS AND RECOMMENDATIONS

Most of the star-image pairs supplied for this study showed no image tear and tended to look Gaussian. The only exception was the star-pair photographed at a 1-msec exposure. Images of stars of unequal magnitude were of unequal width. These facts suggest that the star-image data supplied for this study were unsatisfactory.

Efforts for the immediate future should concentrate on remedying these defects. The Gaussian image appears to be the result of too long an exposure. The unequal image size may be the result either of scattering within the emulsion or of underexposed film. If it is the latter, it will be difficult to solve the problem without going to a longer exposure and thus aggravating the Gaussian-image problem. It may be necessary to investigate other types of emulsion or other means of recording the image. Alternatively, future experiments may have to be restricted to photographing only the brightest stars.

As collateral studies, experiments might be run using artificial sources, e.g., high-intensity lights or lasers, either flown or at ground level, especially if exposure constraints make it difficult to find usable star-pairs covering a wide range of separations.

REFERENCES

1. S. A. Collins, Jr., "Investigation of Laser Propagation Phenomena," Quarterly Technical Report 3432-4, The Ohio State University ElectroScience Laboratory, March, 1973.

2. M. M. Sondhi, "Image Restoration: The Removal of Spatially Invariant Degradations," Proceedings of the IEEE, vol. 60, no. 7, pp. 842-853, July, 1972.

3. J. L. Harris, Sr., "Image Evaluation and Restoration," Journal of the Optical Society of America, vol. 56, no. 5, pp. 569-574, May, 1966.

4. B. L. McGlamery, "Restoration of Turbulence-Degraded Images," Journal of the Optical Society of America, vol. 57, no. 3, pp. 293-297, March, 1967.

UNCLASSIFIED

SECURITY CLASSIFICATION OF THIS PAGE *(When Data Entered)*

REPORT DOCUMENTATION PAGE		READ INSTRUCTIONS BEFORE COMPLETING FORM
1. REPORT NUMBER RADC-TR-73-343	2. GOVT ACCESSION NO. 718030	3. RECIPIENT'S CATALOG NUMBER
4. TITLE *(and Subtitle)* OBSERVATION OF STAR-PAIR IMAGES FOR ESTIMATION OF ISOPLANATIC PATCH SIZE IN THE ATMOSPHERE		5. TYPE OF REPORT & PERIOD COVERED Final Technical Report 12 Feb 73 - 12 Sept 73 6. PERFORMING ORG. REPORT NUMBER
7. AUTHOR(s) Thomas W. Parsons		8. CONTRACT OR GRANT NUMBER(s) F30602-73-C-0284
9. PERFORMING ORGANIZATION NAME AND ADDRESS Federal Scientific Corporation 615 W. 131st St. New York, NY 10027		10. PROGRAM ELEMENT, PROJECT, TASK AREA & WORK UNIT NUMBERS 62301E 1279 07 12790702
11. CONTROLLING OFFICE NAME AND ADDRESS Defense Advanced Research Projects Agency 1400 Wilson Blvd Arlington VA 22209		12. REPORT DATE September 1973 13. NUMBER OF PAGES 57
14. MONITORING AGENCY NAME & ADDRESS*(If different from Controlling Office)* Rome Air Development Center (OCSE) Griffiss Air Force Base, New York 13441		15. SECURITY CLASS. *(of this report)* UNCLASSIFIED 15a. DECLASSIFICATION/DOWNGRADING SCHEDULE N/A

16. DISTRIBUTION STATEMENT *(of this Report)*

Approved for public release; distribution unlimited.

17. DISTRIBUTION STATEMENT *(of the abstract entered in Block 20, if different from Report)*

Same

18. SUPPLEMENTARY NOTES

Monitored by
Donald W. Hanson (OCSE)
RADC, GAFB, NY 13441
AC 315 330-3145

19. KEY WORDS *(Continue on reverse side if necessary and identify by block number)*

Isoplanatic Patch
Seeing
Propagation
Optics

20. ABSTRACT *(Continue on reverse side if necessary and identify by block number)*

An experiment is described which attempts to measure the isoplanatic patch size of the atmosphere as a function of various parameters. Technique constraints and the data analysis procedures used are described and results are discussed. It is shown that the constraints in data collection impaired the data analysis and prevented a measurement of the isoplanatic patch size. Recommendations are given for getting better data in the future.

DD FORM 1 JAN 73 1473 EDITION OF 1 NOV 65 IS OBSOLETE

UNCLASSIFIED

SECURITY CLASSIFICATION OF THIS PAGE *(When Data Entered)*

UNCLASSIFIED

SECURITY CLASSIFICATION OF THIS PAGE(*When Data Entered*)

UNCLASSIFIED

SECURITY CLASSIFICATION OF THIS PAGE(*When Data Entered*)

MISSION
of
Rome Air Development Center

RADC is the principal AFSC organization charged with planning and executing the USAF exploratory and advanced development programs for electromagnetic intelligence techniques, reliability and compatibility techniques for electronic systems, electromagnetic transmission and reception, ground based surveillance, ground communications, information displays and information processing. This Center provides technical or management assistance in support of studies, analyses, development planning activities, acquisition, test, evaluation, modification, and operation of aerospace systems and related equipment.